Shear wave speeds in nearly-incompressible fibrous materials with two fiber families

Running title: Shear wave speeds in fibrous materials

Zuoxian Hou, 1,4 Philip V. Bayly, 1 and Ruth J. Okamoto 1

¹ Department of Mechanical Engineering and Materials Science, Washington University, St. Louis, MO 63130,

USA

Uploaded date: 10/14/2020

Abstract: An analytical and numerical investigation of shear wave behavior in nearly-incompressible,

soft, materials with two fiber families was performed, focusing on the effects of material parameters

and imposed pre-deformations on wave speed. This theoretical study is motivated by the emerging

ability to image shear waves in soft biological tissues by magnetic resonance elastography (MRE). In

MRE, the relationships between wave behavior and mechanical properties can be used to

characterize tissue properties non-invasively. We demonstrate these principles in two material

models, each with two fiber families. One model is a nearly-incompressible linear elastic model that

exhibits both shear and tensile anisotropy; the other is a two-fiber-family version of the widely-used

Holzapfel-Gasser-Ogden (HGO) model, which is nonlinear. Shear waves can be used to probe

nonlinear material behavior using infinitesimal dynamic deformations superimposed on larger, quasi-

static "pre-deformations." In this study, closed-form expressions for shear wave speeds in the HGO

model are obtained in terms of the model parameters and imposed pre-deformations. Analytical

expressions for wave speeds are confirmed by finite element simulations of shear waves with various

polarizations and propagation directions. These studies support the feasibility of estimating the

parameters of an HGO material model noninvasively from measured shear wave speeds.

^a Electronic email: houz@wustl.edu

I. INTRODUCTION

1

2

3

4

5

6

7

8

9

10

11

12

13

14

15

16

17

18

19

20

21

22

23

Magnetic resonance elastography (MRE) is an emerging technique to measure non-invasively the mechanical properties of soft tissue, such as muscle ^{1,2,3}, liver ^{4,5}, and brain ^{6,7}. In MRE, shear waves are generated by small-amplitude external vibrations; the speeds of these waves as they propagate through a region of tissue are determined by its mechanical properties 8,9,10. However, MRE measurements usually involve only small strains from a single experiment, so mechanical properties from MRE are typically limited to linearized, isotropic models of material behavior. Thus, waves must be superimposed on an additional finite deformation in order to study material nonlinearity, and more sophisticated mathematical models are required to explain anisotropic and nonlinear behavior. Many biological soft tissues, such as blood vessels 11,12, cardiac muscle 13,14, and white matter in brain, are structurally anisotropic, composed of one or more families of fibers, each with a dominant direction. The Holzapfel-Gasser-Ogden (HGO) model is a material model that explicitly represents the contributions of fibers to the mechanical response of soft materials under large deformations. The HGO model is straightforward to implement and has been widely used to model fibrous soft tissues 15, 16. In previous work 17, we investigated the relationships between shear wave speeds and material parameters in an HGO model with a single fiber family, which is an example of a nonlinear, transversely isotropic material. However, many biological materials contain two or more fiber families 12,18,19,20,21. In this study we extend our approach to a relatively simple two-fiber-family linear, elastic, orthotropic material as well as to a two-fiber-family HGO model. Complex biological materials are often tested in ex vivo to determine their mechanical properties. However, there are many advantages to being able to characterize such materials in their intact, living condition. The aim of the current paper is to elucidate the relationships between shear wave

speeds and parameters of nonlinear, anisotropic materials with two fiber families, in order ultimately to extend the ability of MRE to characterize these materials *in vivo*.

II. THEORY

A. Shear wave speeds in elastic materials

Speeds of plane waves in a uniform, linear elastic material are obtained from the eigenvalues of the acoustic tensor *Q* ^{22,23}:

$$\rho c^2 \boldsymbol{m} = \boldsymbol{Q}(\boldsymbol{n}) \cdot \boldsymbol{m} \tag{1}$$

where ρc^2 is the eigenvalue of the acoustic tensor Q, ρ is the density of material, c is the wave speed, n is the propagation direction of the wave, and m, the eigenvector of the acoustic tensor, is the polarization direction vector of the plane wave. The acoustic tensor Q corresponding to a specific propagation direction, n, is calculated from Eq. (2) 22,23 below,:

$$Q = n \cdot A \cdot n \tag{2}$$

Here A is a fourth-order elasticity tensor which describes the relationship of the incremental stress tensor, $\tilde{\sigma}$, and the incremental strain tensor, $\tilde{\varepsilon}$, specifically: $\tilde{\sigma} = A \cdot \tilde{\varepsilon}$ In Cartesian coordinates this relationship can be written in indicial notation, $\tilde{\sigma}_{pi} = A_{piqj}\tilde{\varepsilon}_{qj}$. For nonlinear models with constitutive behavior defined by the strain energy density function, W(F), the components of the elasticity tensor can be obtained from the relationship:

$$A_{piqj} = F_{p\alpha}F_{q\beta}\frac{\partial^2 W}{\partial F_{i\alpha}\partial F_{j\beta}}$$
 (3)

where \mathbf{F} is the deformation gradient tensor (which accounts for the effects of pre-deformation 43 ^{22,23}). For finite strain, \mathbf{A} is a function of the deformation state defined by \mathbf{F} , therefore \mathbf{A} and \mathbf{Q} can

describe small-amplitude wave motion superimposed on a larger initial deformation, which we willrefer to as "pre-deformation."

Since the acoustic tensor, \mathbf{Q} , depends on \mathbf{n} , the wave speeds also depend on \mathbf{n} . In general anisotropic materials there are three distinct eigenvalues (wave speeds) and three corresponding eigenvectors (polarization directions), which means there may be three plane waves that propagate in the same direction. However, material symmetries and constraints can reduce the number of possible distinct wave speeds.

In an isotropic linear elastic material with shear modulus, μ and bulk modulus, K, the acoustic tensor is the same for all propagation directions, and only two wave speeds exist: one longitudinal and one transverse (shear). Longitudinal waves in isotropic materials have speed $c^2 = (K + \frac{4\mu}{3})/\rho$ and polarization parallel to the propagation direction (m = n); shear waves have $c^2 = \mu/\rho$ and polarization direction $m \perp n$. In an isotropic, incompressible linear elastic material, the bulk modulus and longitudinal wave speed become infinite, and only one material parameter, μ , and one finite (shear) wave speed remains to be determined.

In anisotropic materials, three distinct wave speeds and three corresponding polarization vectors are obtained from the eigenvalue problem in Eq. (1). In transversely isotropic and orthotropic materials, the three plane wave modes are typically known as "pure shear" (or "slow"), "quasi-shear" (or "fast"), and "quasi-longitudinal" waves ²⁵.

B. Orthotropic Material Models

1. Linear elastic orthotropic materials

In a linear elastic material, the generalized Hooke's law,

$$\sigma_{ij} = A_{ijkl} \epsilon_{kl} \,, \tag{4}$$

describes the relationship between the infinitesimal strain tensor ϵ_{kl} and the stress tensor σ_{ij} . A general fourth-order tensor has 81 components, but in the elasticity tensor this number is reduced to 21 by general symmetry constraints.

Using Voigt notation ²⁵, a 6×6 symmetric compliance matrix, S, and corresponding stiffness matrix, $C = S^{-1}$, compactly capture the stress-strain relationships in the elasticity tensor. For an orthotropic material, these matrices can be written in terms of nine constants (three Young's moduli, three shear moduli and three Poisson's ratios).

If the material is incompressible, there are three additional constraints relating the components of the elasticity tensor, and the compliance and stiffness matrices. In this case, the Poisson's ratios can be expressed as

77
$$v_{ij} = \frac{1}{2}E_i\left(\frac{1}{E_i} + \frac{1}{E_j} - \frac{1}{E_k}\right) \quad (k \neq i \neq j, i, j = 1, 2, 3)$$
 (5)

Thus, the number of independent constants is reduced to six in the general, incompressible, orthotropic case.

2. Model 1: Linear elastic, nearly-incompressible, orthotropic material model

We can illustrate wave behavior in fiber-reinforced materials using a linear, elastic, orthotropic material model derived from a strain energy density function, $W = W_{iso} + W_{aniso} + W_{vol}$. The

volumetric component of the strain energy function can be described in terms of bulk modulus, K, and the volume ratio, $J = \det F$:

$$W_{vol} = \frac{K}{2}(J-1)^2.$$
(6)

The isochoric (volume-conserving) component contains contributions from an isotropic term,

$$W_{iso} = \frac{\mu}{2}(\bar{I}_1 - 3),\tag{7}$$

and an anisotropic component due to fiber stretch and shear in the plane containing fibers.

89
$$W_{aniso} = \frac{\mu}{2} \left[\zeta_A (\bar{I}_4 - 1)^2 + \eta_A \bar{I}_5^* + \zeta_B (\bar{I}_6 - 1)^2 + \eta_B \bar{I}_7^* + \zeta_{AB} (\bar{I}_4 - 1) (\bar{I}_6 - 1) \right]$$
(8)

- Here \bar{I}_1 is the modified first invariant defined by $\bar{I}_1 = J^{-2/3}I_1$, $(J = \det \mathbf{F})$, where I_1 is the first
- 91 invariant (trace) of the Cauchy-Green strain tensor \boldsymbol{C} . The modified pseudo-invariants are $\bar{I}_4 =$
- 92 $J^{-2/3}I_4$, where $I_4 = \boldsymbol{a}_A \cdot \boldsymbol{C} \boldsymbol{a}_A$; $\bar{I}_5^* = J^{-\frac{4}{3}}I_5^*$, where $I_5^* = I_5 I_4^2$, and $I_5 = \boldsymbol{a}_A \cdot \boldsymbol{C}^2 \boldsymbol{a}_A$; $\bar{I}_6 = J^{-2/3}I_6$,
- 93 where $I_6 = a_B \cdot C a_B$; and $\bar{I}_7^* = J^{-\frac{4}{3}} I_7^*$, where $I_7^* = I_7 I_6^2$, and $I_7 = a_B \cdot C^2 a_B$ (a_A and a_B are the
- 94 initial fiber directions). The pseudo-invariants I_4 and I_6 (invariant under rotations about a_A and a_B
- 95 respectively) are the squared stretch ratios in the corresponding fiber directions, and I_5^* and I_7^*
- 96 represent the squared shear strains in planes parallel to those directions.
- The linear, orthotropic material model was derived by using Eq. (3) with $\mathbf{F} = \mathbf{I}$, to obtain the
- elasticity tensor in terms of the parameters μ , ζ_A , ζ_B , ζ_{AB} , η_A , and η_B . In this model, the
- parameters ζ_A and ζ_B describe additional strain energy due to tensile stiffness contributed by the two
- 100 fiber families, and ζ_{AB} quantifies additional strain energy due to interactions between the fiber
- 101 families. The parameters η_A and η_B describe additional strain energy due to shear in the planes
- 102 containing the fibers. Thus non-zero ζ_A , ζ_B , ζ_{AB} , model tensile anisotropy, and non-zero η_A , and

 η_B model shear anisotropy. If these parameters all were to vanish, the material model would become 104 isotropic.

3. Model 2: Nonlinear model: the two-fiber-family HGO model

The HGO model, which is widely used in soft biological tissues, is described in detail in $^{\circ}$ reference²⁶. The HGO model represents a hyperelastic material reinforced by families of fibers, each with a dominant direction and distribution parameter. For multiple fiber-family models, each additional fiber family can be modeled by adding contributions from $I_{4i} = a_{0i} \cdot C \cdot a_{0i}$ to the strain energy, as follows:

111
$$W = W_{iso} + W_{aniso} + W_{vol}$$
, where $W_{vol} = \frac{K}{2}(J-1)^2$, $W_{iso} = \frac{\mu}{2}(\bar{I}_1 - 3)$

112
$$W_{aniso\ HGON} = \sum_{i} \frac{k_1}{2k_2} \left[exp\left(k_2 \bar{E}_i^2\right) - 1 \right]; \quad \bar{E}_i = \kappa \bar{I}_1 + (1 - 3\kappa)\bar{I}_{4i} - 1, \ for\ \bar{I}_{4i} > 1.$$
 (9)

where k_1 and k_2 respectively describes the initial slope and the nonlinearity of strain-stress curve, κ is the fiber angle dispersion parameter, varying from $\kappa=0$ (all fibers within a fiber family perfectly aligned in a single orientation) to $\kappa=1/3$ (no preferred orientation).

The linear orthotropic model is a minimal, linear elastic model that can describe materials in which fibers contribute both shear and tensile anisotropy in the reference configuration, but which is not designed to describe behavior under large deformations. In contrast, in the HGO material model, fiber reinforcement does not affect slow shear wave behavior in the undeformed configuration. However, the HGO model is well suited for describing behavior under large deformations. As a result, it is one of the most widely used models of fibrous soft tissues. We wish to study both models, because both small and large deformations are important in biomechanics, and can possibly be interrogated by shear waves.

C. Computational domain and boundary conditions

125

146

147

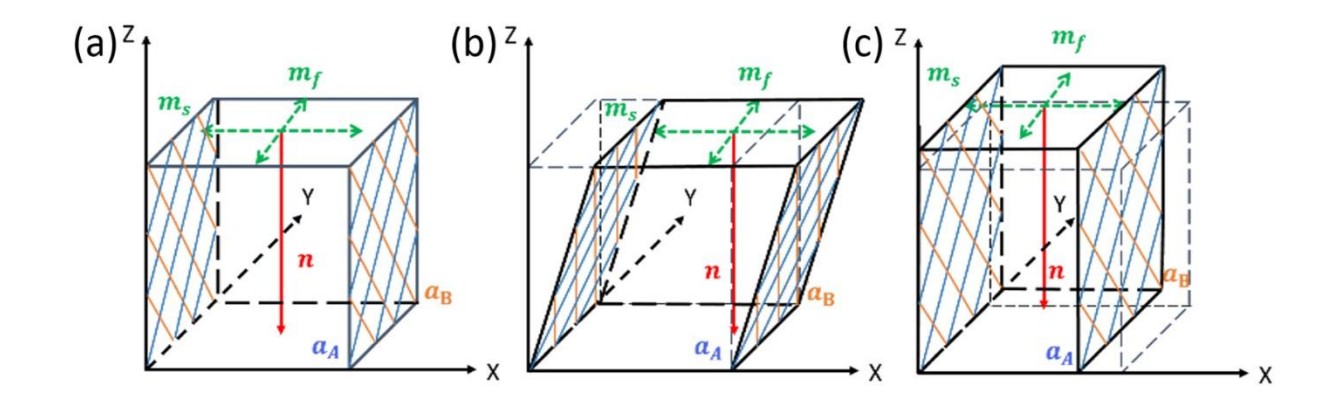
126 We consider the case in which the two fiber families are mechanically equivalent. In this case for 127 the linear elastic model, there are only four "intrinsic" material parameters (properties of the matrix and fibers: μ , $\zeta_A=\zeta_B=\zeta_0$, $\zeta_{AB}=\zeta_1$, $\eta_A=\eta_B=\eta_0$). For the HGO model with two 128 129 mechanically equivalent fiber families, the number of intrinsic parameters is also four: μ , k_1 , k_2 , κ . In 130 both models, a fifth independent parameter which affects the mechanical response is the fiber angle, ϕ_0 , defined in this paper to be the angle between each fiber direction and their bisecting axis 131 132 (half the angle between fiber axes). Finite element simulations were performed using COMSOL Multiphysics (v 5.4, COMSOL Inc., 133 134 Burlington, MA) for both the linear elastic and HGO models, to confirm analytical predictions and illustrate the effects of material parameters and pre-deformation on shear wave behavior. The 135 136 geometry of the computational domain is a cube (50×50×50 mm³) depicted in Figure 1. The default 137 parameters for the linear elastic model, unless otherwise noted, are as follows: initial isotropic shear modulus, $\mu_0=1$ kPa; tensile anisotropy $\zeta_0=2$; shear anisotropy $\eta_0=2$; interaction factor $\zeta_1=1$ 138 139 0; The default parameters for the HGO model, unless otherwise noted, are as follows: predeformation $\gamma_{XZ}=0.2$; initial isotropic shear modulus, $\mu_0=1$ kPa; initial anisotropy ratio, 140 $k_1/\mu_0=2$; nonlinearity parameter, $k_2=5$; fiber dispersion parameter, $\kappa=1/12$; and ratio of bulk 141 modulus to initial shear modulus, $K/\mu_0 = 10^4$ (the effect of assumed bulk modulus on shear wave 142 speeds for $10^4 < \frac{K}{\mu_0} < 10^6$ was investigated in a subset of simulations and found to be negligible). 143 144 The density $\rho = 1000 \text{ kg/m}^3$ in both cases. Default parameters for both models are summarized in 145 Table I.

Table I. Default parameters of linear elastic model and HGO model in numerical simulation.

Linear elastic mod	del	HGO model	HGO model			
$\mu_0(kPa)$	1	$\mu_0(kPa)$	1			
ζ_0	2	k_1/μ_0	2			
η_0	2	k_2	5			
ζ_1	0	κ	1/12			
K/μ_0	10^4					
$\rho(kg/m^3)$	1000					
f(Hz)	200					

The HGO model is implemented in COMSOL by defining a hyperelastic material model with properties specified by a user-defined strain energy density function. The isochoric and volumetric components of the strain energy density function in Eq. (9) are entered separately.

Local frequency estimation (LFE) ²⁷ was used to estimate wavelength in simulated displacement fields. LFE, which is based on the successive application of a bank of spatial filters, provides an estimated wave speed within each "voxel" in a central region of interest. The mean value and standard deviation of voxel-wise estimates are reported for each simulation ^{27, 28}. In this study, the LFE parameters were $\rho_0 = 1/L$ (L=50 mm) for the central spatial frequency of the first filter and $N_f = 11$ for the number of filters.



160

161

162

163

164

165

167

168

Figure 1. Geometry of computational domain. Green dashed lines represent harmonic excitation in two perpendicular directions (X- and Y-) on the top surface. Red arrows show the propagation direction parallel to the Z-axis. Blue and orange solid lines show dominant directions of two fiber families, where the fiber angle $\phi_0 = \pi/4$ in this example. (a) Undeformed geometry. (b) Simple shear in the XZ-plane. (c) Compression in the X-direction, which also causes stretch in the Y- and Z- directions.

166 III. RESULTS: SHEAR WAVE SPEEDS IN LINEAR ELASTIC AND HGO TWO-

FIBER MODELS

- A. Model 1: Incompressible, orthotropic, linear elastic material model
- 169 1. Compliance matrix in terms of model parameters
- The compliance matrix, S, can be expressed compactly as a "normal compliance" matrix (R) and
- 171 "shear compliance" matrix (*T*). In the limit of incompressibility (infinite bulk modulus) we obtain:

172
$$S = \begin{bmatrix} R & 0 \\ 0 & T \end{bmatrix}$$
, where $R = \begin{bmatrix} \frac{A}{\mu Z} & \frac{-(A+B)}{2\mu Z} & \frac{-(A-B)}{2\mu Z} \\ \frac{-(A+B)}{2\mu Z} & \frac{A+2B+C}{4\mu Z} & \frac{A-C}{4\mu Z} \\ \frac{-(A-B)}{2\mu Z} & \frac{A-C}{4\mu Z} & \frac{A-2B+C}{4\mu Z} \end{bmatrix}$ and

173
$$T = \begin{bmatrix} \frac{1}{2\mu(1+2\eta_0\cos^22\phi_0 + (2\zeta_0 - \zeta_1)\sin^22\phi_0)} & 0 & 0\\ 0 & \frac{1}{2\mu(1+2\eta_0\cos^2\phi_0)} & 0\\ 0 & 0 & \frac{1}{2\mu(1+2\eta_0\sin^2\phi_0)} \end{bmatrix}$$

where
$$A = 1 + 2\eta_0 \sin^2 2\phi_0 + (2\zeta_0 + \zeta_1)\cos^2 2\phi_0$$
, $B = \frac{1}{3}(2\zeta_0 + \zeta_1)\cos 2\phi_0(1 + \zeta_0)\cos 2\phi_0$

175
$$2\cos^2 2\phi_0$$
), and $C = 3 + 2\zeta_0 + \zeta_1$, where $Z = AC - B^2$.

Elements of the compliance matrix are compared to the classical elastic parameters (Young's moduli, shear moduli, and Poisson's ratios) in Table II.

Table II. Comparison of classical elastic parameters to elements of compliance matrix inorthotropic, linear elastic model.

Parameter	Element	Parameter	Element	Parameter	Element		
E_1	$\frac{\mu Z}{A}$	$ u_{12}$	$\frac{A+B}{2A}$	$ u_{21}$	$\frac{2(A+B)}{A+2B+C}$		
E_2	$\frac{4\mu Z}{A+2B+C}$	$ u_{13}$	$\frac{A-B}{2A}$	$ u_{31}$	$\frac{2(A-B)}{A-2B+C}$		
E_3	$\frac{4\mu Z}{A - 2B + C}$	$ u_{23}$	$\frac{-(A-C)}{A+2B+C}$	v_{32}	$\frac{-(A-C)}{A-2B+C}$		
Parameter		Element of compliance matrix					
G_{23}		$\mu(1 + 2\eta_0 \cos^2 2\phi_0 + (2\zeta_0 - \zeta_1) \sin^2 2\phi_0)$					
G ₃₁		$\mu(1+2\eta_0\cos^2\phi_0)$					
G_{12}		$\mu(1+2\eta_0\sin^2\phi_0)$					

For the special case where $\phi_0=0$ (two fiber families are parallel, Figure 2a), the compliance matrix is identical to that of an incompressible transversely isotropic (ITI) model, in which

184
$$\mathbf{R} = \begin{bmatrix} \frac{1+2\zeta_0+\zeta_1}{\mu[3+4(2\zeta_0+\zeta_1)]} & \frac{-(1+4\zeta_0+2\zeta_1)}{2\mu[3+4(2\zeta_0+\zeta_1)]} & \frac{-1}{2\mu[3+4(2\zeta_0+\zeta_1)]} \\ \frac{-(1+4\zeta_0+2\zeta_1)}{2\mu[3+4(2\zeta_0+\zeta_1)]} & \frac{1+2\zeta_0+\zeta_1}{\mu[3+4(2\zeta_0+\zeta_1)]} & \frac{-1}{2\mu[3+4(2\zeta_0+\zeta_1)]} \\ \frac{-1}{2\mu[3+4(2\zeta_0+\zeta_1)]} & \frac{-1}{2\mu[3+4(2\zeta_0+\zeta_1)]} & \frac{1}{\mu[3+4(2\zeta_0+\zeta_1)]} \end{bmatrix} \text{ and } \mathbf{T} = \begin{bmatrix} \frac{1}{2\mu(1+2\eta_0)} & 0 & 0 \\ 0 & \frac{1}{2\mu(1+2\eta_0)} & \frac{1}{2\mu} \\ 0 & 0 & \frac{1}{2\mu} \end{bmatrix}.$$

- In this special case, there is no effect of tensile anisotropy in the shear compliance matrix (T),
- and no effect of shear anisotropy in the normal compliance matrix (\mathbf{R}) .
- When $\phi_0 = \pi/4$ (when the two fibers are perpendicular, Figure 2b), the compliance matrix
- describes another type of transversely isotropic material,

$$\mathbf{R} = \begin{bmatrix} \frac{1+2\eta_0}{\mu(1+2\eta_0)(3+2\zeta_0+\zeta_1)} & \frac{-(1+2\eta_0)}{2\mu(1+2\eta_0)(3+2\zeta_0+\zeta_1)} & \frac{-(1+2\eta_0)}{2\mu(1+2\eta_0)(3+2\zeta_0+\zeta_1)} \\ \frac{-(1+2\eta_0)}{2\mu(1+2\eta_0)(3+2\zeta_0+\zeta_1)} & \frac{4+2\eta_0+2\zeta_0+\zeta_1}{4\mu(1+2\eta_0)(3+2\zeta_0+\zeta_1)} & \frac{2\eta_0-2-2\zeta_0-\zeta_1}{4\mu(1+2\eta_0)(3+2\zeta_0+\zeta_1)} \\ \frac{-(1+2\eta_0)}{2\mu(1+2\eta_0)(3+2\zeta_0+\zeta_1)} & \frac{2\eta_0-2-2\zeta_0-\zeta_1}{4\mu(1+2\eta_0)(3+2\zeta_0+\zeta_1)} & \frac{4+2\eta_0+2\zeta_0+\zeta_1}{4\mu(1+2\eta_0)(3+2\zeta_0+\zeta_1)} \end{bmatrix} \text{ and }$$

190
$$T = \begin{bmatrix} \frac{1}{2\mu(1+2\zeta_0-\zeta_1)} & 0 & 0\\ 0 & \frac{1}{2\mu(1+\eta_0)} & 0\\ 0 & 0 & \frac{1}{2\mu(1+\eta_0)} \end{bmatrix}.$$

193

194

In this case, both **R** and **T** contain all the model parameters.

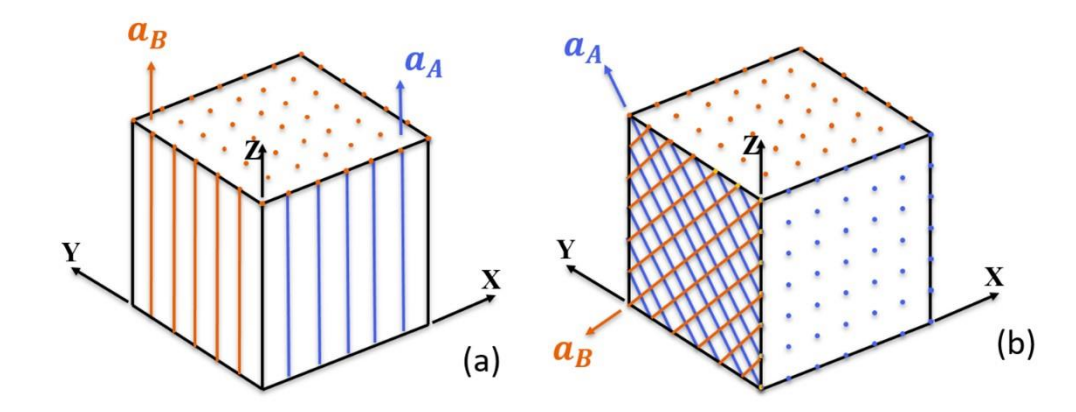


Figure 2. Two special (transversely isotropic) cases of the linear, orthotropic model defined by fiber axes (a_A, a_B) : (a) Fiber axes are parallel $(\phi_0 = 0^\circ)$; (b) Fiber axes are perpendicular $(\phi_0 = \pi/4)$.

2. Shear wave behavior in the incompressible, linear elastic orthotropic model

In the incompressible limit (as $K \to \infty$) the longitudinal wave speed becomes infinite, and two shear wave modes can be separated into "slow" (pure shear) and "fast" (quasi-shear) shear waves with perpendicular polarization directions. The slow and fast polarization directions can be calculated from the propagation direction \boldsymbol{n} and the "symmetry axis", \boldsymbol{a} , which is normal to the plane spanned by the two fiber directions. For propagation in the \boldsymbol{Z} –direction ($\boldsymbol{n}=\pm\boldsymbol{k}$), the acoustic tensor \boldsymbol{Q} below is expressed in terms of model parameters in this situation (two fibers aligned on YZ plane):

203
$$\mathbf{Q} = \begin{bmatrix} \mu[1 + 2\eta_0 \cos^2 \phi_0] & 0 & 0\\ 0 & \mu[1 + 2\eta_0 \cos^2 2\phi_0 + (2\zeta_0 - \zeta_1) \sin^2 2\phi_0] & 0\\ 0 & 0 & \infty \end{bmatrix} (10)$$

where ϕ_0 is the angle between two fibers and Z-axis. In the absence of boundary effects, harmonic excitation in the slow polarization direction m_s generates only slow shear waves, and excitation in the fast polarization direction m_f only generates fast shear waves. Figure 3 illustrates the slow and fast polarization directions in an orthotropic material.

In the undeformed configuration, the slow shear wave speed increases with μ and η_0 but is not affected by ζ_0 . In contrast, the fast shear wave speed increases with μ and ζ_0 , but is not sensitive to η_0 . For the specific case in which the shear waves propagate in the Z-direction, relatively simple expressions for shear wave speeds can be found in terms of material parameters:

$$c_s^{ortho} = \left(\sqrt{\frac{\mu}{\rho}}\right)\sqrt{1 + 2\eta_0 \cos^2 \phi_0} \tag{11}$$

213
$$c_f^{ortho} = \left(\sqrt{\frac{\mu}{\rho}}\right) \sqrt{1 + 2\eta_0 \cos^2 2\phi_0 + (2\zeta_0 - \zeta_1) \sin^2 2\phi_0}$$
 (12)

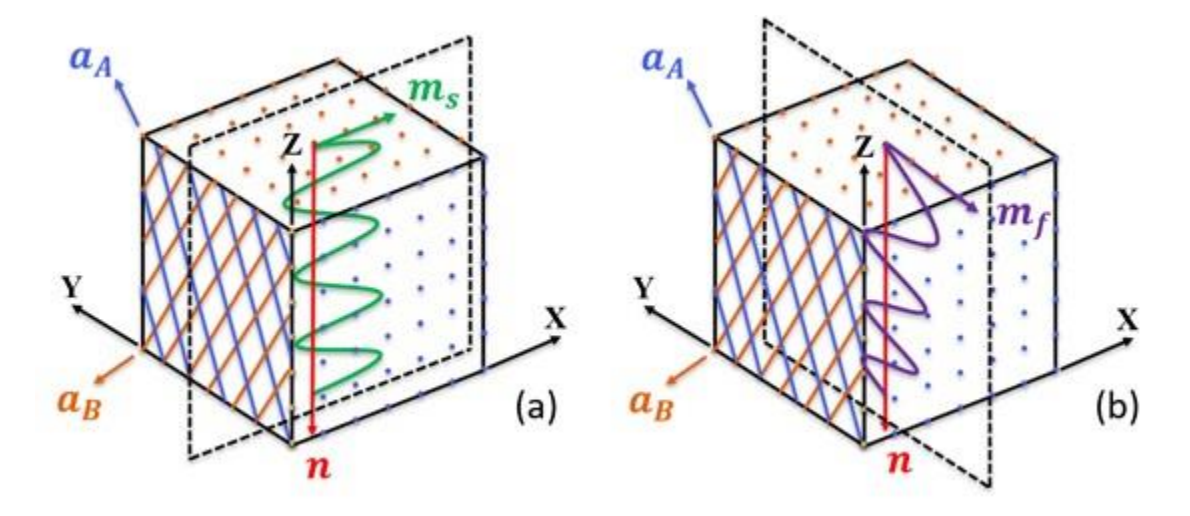


Figure 3. Wave propagation with two polarization directions in the two-fiber-family, linear elastic, orthotropic material. a_A and a_B are the fiber axes. (a) A pure shear ("slow") wave is induced by harmonic shear displacement in the slow polarization direction, m_s . (b) A quasi-shear ("fast") wave arises from harmonic shear displacement in the fast polarization direction, m_f .

These analytical predictions are illustrated in Figure 4 along with corresponding estimates from FE simulation. For other propagation directions, more complicated expressions can be calculated from the general relationships between the acoustic tensor, its eigenvalues (wave speeds), and the mechanical parameters of the undeformed baseline model. We emphasize that these results apply to material that is incompressible or nearly-incompressible. In Figure 4(h), the fast shear wave speed is independent of the fiber angle because this particular example depicts the special case in which shear anisotropy and tensile anisotropy parameters are equal ($\eta_0 = \zeta_0$). In Figure 5, the general effects of shear and tensile anisotropy are illustrated using two different combinations of η_0 , ζ_0 .

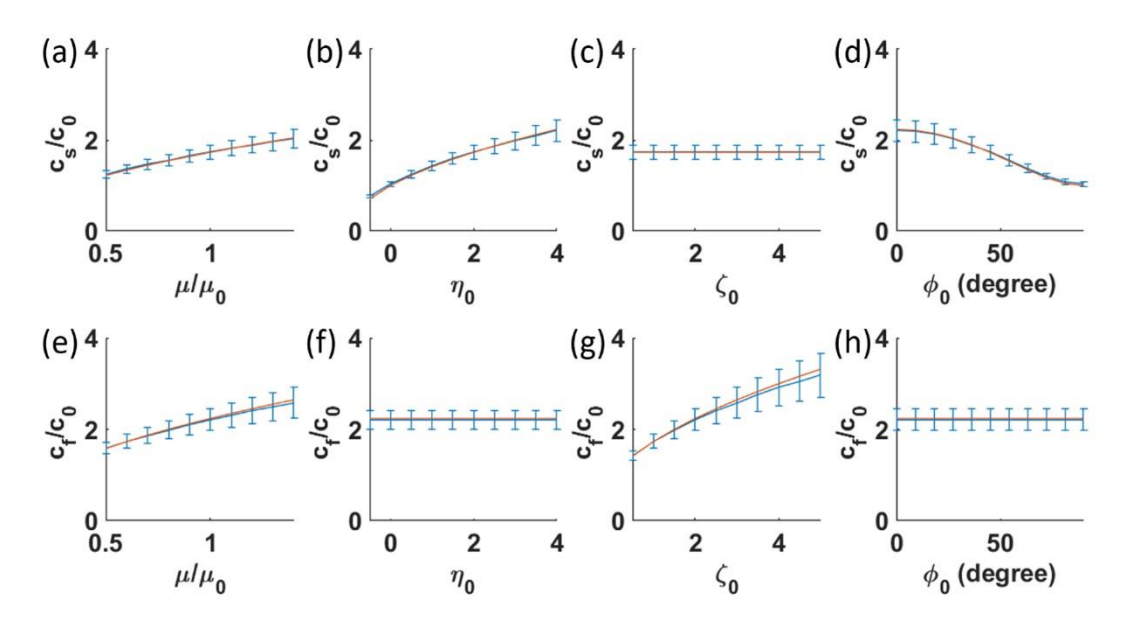


Figure 4. Relationships between pure shear ("slow") and quasi-shear ("fast") shear wave speeds and parameters $(\mu, \eta_0, \zeta_0, \phi_0)$ of the linear elastic, orthotropic material model. (a-d) Relationships between "slow" shear wave speeds and model parameters $(\mu, \eta_0, \zeta_0, \phi_0)$. (e-h) Relationships between "fast" shear wave speeds and model parameters. Blue bars denote mean \pm standard deviations of voxelwise estimates of wave speed from LFE of simulation; orange curves show analytical results. Default parameters are $\mu_0 = 1000 \ Pa, \frac{\mu}{\mu_0} = 1, \eta_0 = 2, \zeta_0 = 2$, and $\phi_0 = \pi/4$.

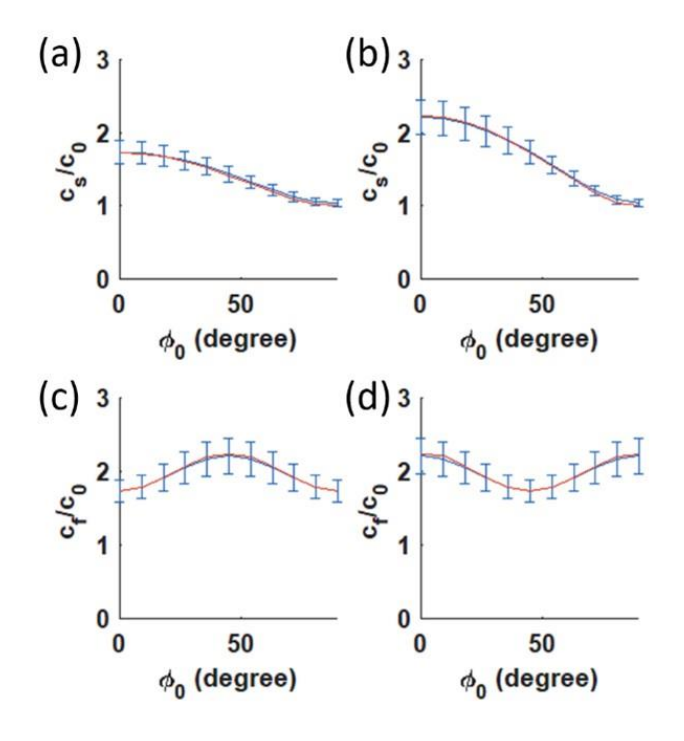


Figure 5. Relationships between slow and fast shear wave speeds and fiber angle ϕ_0 in the linear elastic orthotropic model for combinations of unequal anisotropy parameters. (a, c) Slow and fast shear wave speeds vs fiber angle for tensile anisotropy greater than shear anisotropy ($\eta_0 = 1, \zeta_0 = 2$) (b, d) Slow and fast shear wave speeds and fiber angle for shear anisotropy greater than tensile anisotropy ($\eta_0 = 2, \zeta_0 = 1$). Blue bars denote mean \pm standard deviations of voxelwise estimates of wave speed from LFE of simulation; orange curves show analytical results. Default parameters: Default parameters are $\mu_0 = 1000 \ Pa, \frac{\mu}{\mu_0} = 1$.

B. Model 2: comparison between simulation and theory in the HGO model

1. Elements of the linearized compliance matrix in terms of HGO model parameters

The HGO model can also be linearized about the reference configuration to obtain elements of an orthotropic stiffness matrix expressed as functions of HGO model parameters (Table III). In this linearization, the fibers are assumed to resist an infinitesimal amount of axial compression (as though they are under an infinitesimal amount of pre-stretch). In the original HGO model, fibers

cannot resist compressive axial loading; this is a strong nonlinearity that we avoid here, forsimplicity.

Table III. Comparison of classical elastic parameters to elements of compliance matrix in the HGO

253 model

Parameter	Element	Parameter	Element	Parameter	Element		
E_1	$\frac{\mu Z}{A}$	$ u_{12}$	$\frac{A+B}{2A}$	$ u_{21}$	$\frac{2(A+B)}{A+2B+C}$		
E_2	$\frac{4\mu Z}{A+2B+C}$	$ u_{13}$	$\frac{A-B}{2A}$	$ u_{31}$	$\frac{2(A-B)}{A-2B+C}$		
E_3	$\frac{4\mu Z}{A-2B+C}$	v_{23}	$\frac{-(A-C)}{A+2B+C}$	$ u_{32}$	$\frac{-(A-C)}{A-2B+C}$		
Parameter		Element of compliance matrix					
G_{23}		$\mu \left(1 + 2(1 - 3\kappa)^2 \frac{k_1}{\mu} \sin^2 2\phi_0\right)$					
G ₃₁		μ					
G ₁₂		μ					

where
$$A = 1 + 2(1 - 3\kappa)^2 \frac{k_1}{\mu} \cos^2 2\phi_0$$
, $B = \frac{2}{3}(1 - 3\kappa)^2 \frac{k_1}{\mu} \cos^2 2\phi_0$ (1 + 2 cos² 2 ϕ_0)

256
$$C = 3 + 2(1 - 3\kappa)^2 \frac{k_1}{\mu}$$
, and $Z = AC - B^2$.

2. Shear wave behavior in the HGO model – reference configuration

As in the undeformed model, for waves propagating in the Z-direction, the closed-form expressions for fast and slow shear wave speed in the linearized HGO model (under no predeformation) can be summarized as

$$c_s^{HGO} = \sqrt{\frac{\mu}{\rho}} \tag{13}$$

$$c_f^{HGO} = \left(\sqrt{\frac{\mu}{\rho}}\right) \sqrt{1 + 2(1 - 3\kappa)^2 \frac{k_1}{\mu} \sin^2 2\phi_0}.$$
 (14)

Analytical expressions and simulations were used to illustrate the effects of the HGO parameters (Figure 6). In the undeformed case, slow shear wave speeds only varied with the initial shear modulus μ , fast shear wave speeds increased with μ and k_1 , but decreased with κ . Estimates of wave speeds in simulations agree well with the analytical predictions. In the HGO model, fast shear wave speeds exhibit a marked sinusoidal relationship with fiber angle (Figure 6h), but slow shear wave speeds are insensitive to fiber orientation (Figure 6d). This insensitivity is because in the HGO model in the reference configuration fibers add stiffness in tension but not in shear.

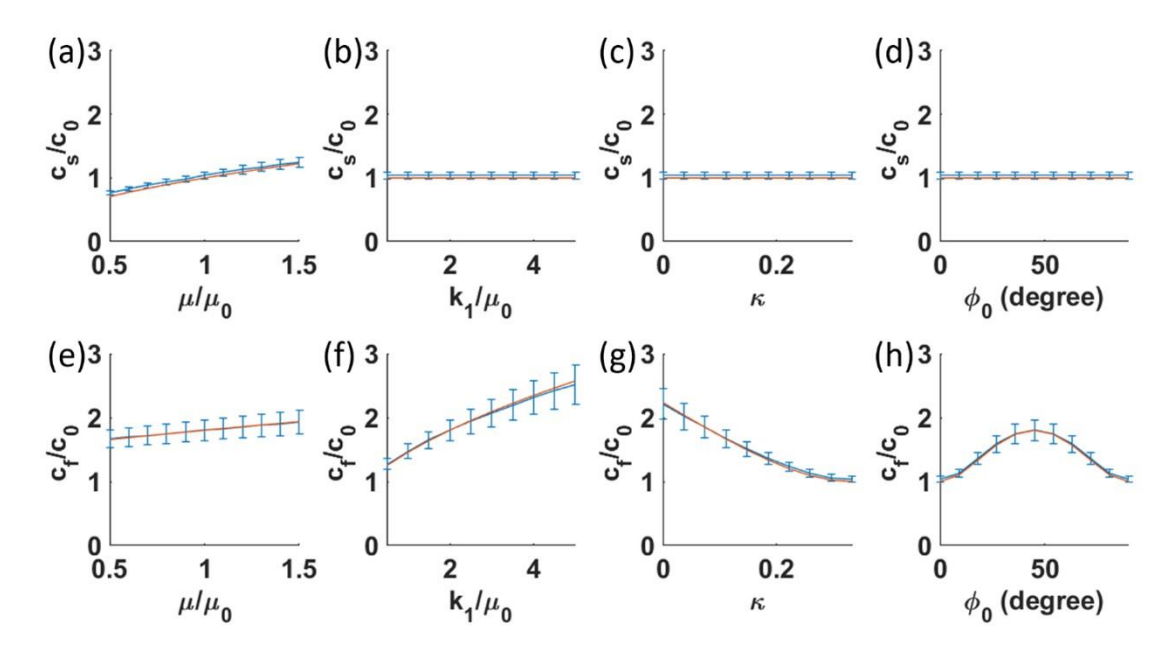


Figure 6. Relationships between slow and fast shear wave speeds and parameters $(\mu, k_1, \kappa, \phi_0)$ of the HGO model in its undeformed configuration $(\lambda = 1)$. (a-d) Relationships between "slow" shear wave speeds and parameters $(\mu, k_1, \kappa, \phi_0)$ of the HGO model.(e-h) Relationships between "fast" shear wave speeds and model parameters. Blue bars denote mean \pm standard deviations of voxelwise estimates of wave speed from LFE of simulation; orange curves show analytical results. Default parameters: $\mu_0 = 1000 \ Pa$, $\frac{\mu}{\mu_0} = 1$, $k_1/\mu_0 = 2$, $\kappa = 1/12$, $k_2 = 5$, $\gamma_{XZ} = 0$.

3. Shear wave behavior in the HGO model – deformed configuration

Simulated displacement fields due to slow and fast shear waves after different pre-deformations are applied are shown in Figure 7. Fibers are aligned with the YZ-plane. The entire domain is deformed by compression in X-direction and simple shear in XZ-plane, leading to changes in the shear wave speeds.

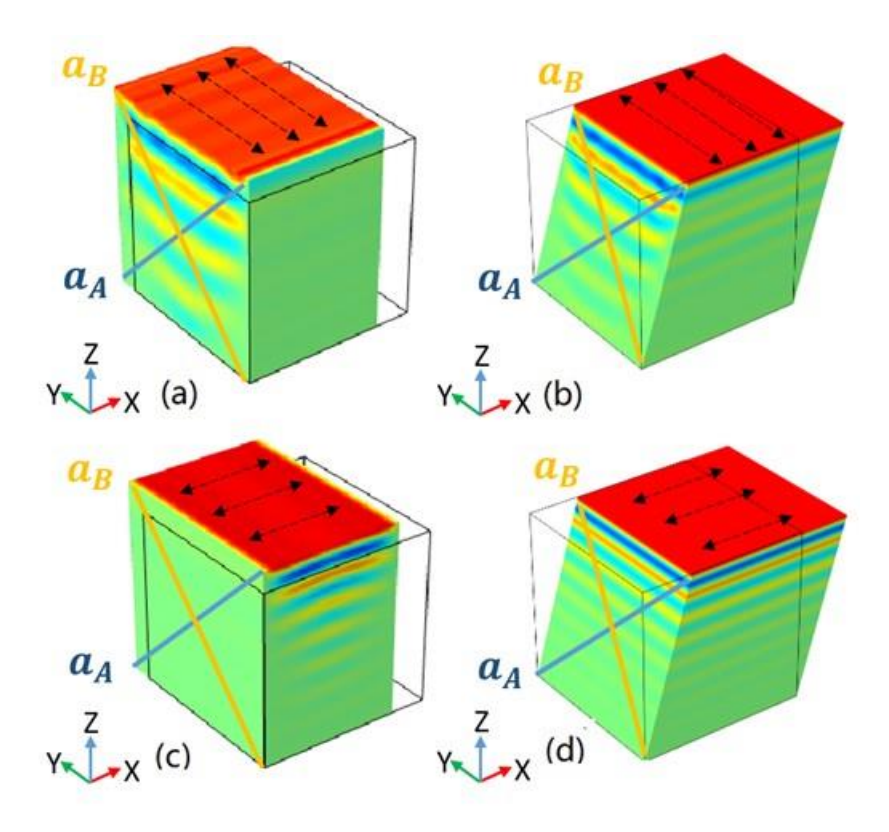


Figure 7. HGO model. Displacement fields due to slow and fast shear waves superimposed on two types of pre-deformation. Black dashed lines represent harmonic excitation in the specified direction on the top surface, a_A and a_B are fiber axes. (a,c) Fast and slow small-amplitude shear waves superimposed on finite compression in the X-direction $(1 - \lambda = 0.2)$. (b,d) Fast and slow small-amplitude shear waves superimposed on finite pure shear deformation in XZ-plane ($\gamma_{XZ} = 0.2$). The effects of imposed compression in the X-direction, (stretch ratio λ), imposed shear in the

XZ —plane (shear γ_{XZ}), and fiber angle, ϕ_0 , on shear wave speeds in the HGO model are quantified in Figure 8. In the deformed configurations, both slow and fast shear wave speeds increase with increasing compression, λ , and shear, γ_{XZ} .

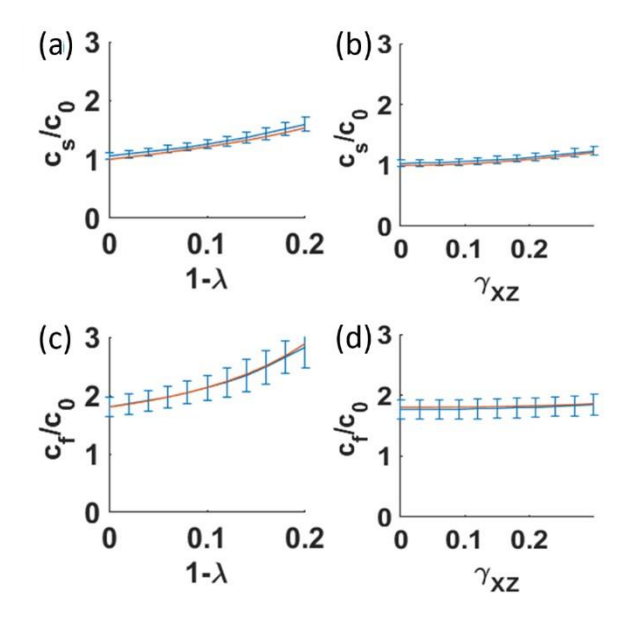


Figure 8. HGO model. (a, c) Relationships between slow/fast shear wave speeds and compressive stretch ratio λ , for waves superimposed on finite compression in the X-direction (and accompanying stretch in Y- and Z-directions). (b, d) Relationships between slow and fast shear wave speeds and shear deformation, γ_{XZ} , for waves superimposed on finite shear in the XZ-plane. Blue bars denote mean \pm standard deviations of voxelwise wave speed estimates from LFE of simulation; orange curves show analytical results. Default parameters: $\mu_0 = 1000 \ Pa$, $\frac{\mu}{\mu_0} = 1$, $k_1/\mu_0 = 2$, $\kappa = 1/12$, $k_2 = 5$, $\lambda = 1$, $\gamma_{XZ} = 0$, and $\phi_0 = \pi/4$.

IV. DISCUSSION

Shear wave behavior was investigated analytically and numerically in two models of fibrous, soft materials: an orthotropic, linear elastic model, and the HGO two-fiber-family model. Analytical predictions of the effects of mechanical parameters on shear wave speeds were confirmed by simulation. Analytical and numerical predictions of shear wave speeds after pre-deformations (pure shear, compression), also agree well and illustrate the effects of nonlinearity on wave behavior.

In each model, the strain-stress relationship can be captured by four intrinsic material parameters (properties of the matrix and fiber components), along with the corresponding fiber orientation ϕ_0 . For materials with the same matrix and fiber properties, the wave propagation direction relative to fiber orientation is important in determining wave speed. For example, in the special cases considered in this paper, propagation is in the Z-direction and fibers are in the YZ-plane. In the linear elastic model, as the fiber angle ϕ_0 (which is also the angle between propagation direction and fiber direction) increases from 0 to 90 degrees, the slow shear wave speed decreases monotonically (Figures 4-5). In the linear elastic model, the effect on fast shear wave speed of the fiber angle varies according to the relative magnitude of shear and tensile anisotropy (Figures 4-5). In the HGO model, in the undeformed configuration slow shear waves are not affected by the fiber angle, but fast shear wave speeds exhibit a nearly sinusoidal variation with fiber angle (Figure 6), maximal at $\phi_0 = \pi/4$.

In the HGO model, which is explicitly nonlinear, finite pre-deformation (such as imposed shear deformation or compression) also affects wave speeds (Figure 7 and Figure 8). There are two points which distinguish the linear elastic model and the nonlinear HGO model: (1) The HGO model does not capture the effect of fibers on slow shear wave speed in the reference configuration (the linear orthotropic model is better suited for that purpose); (2) the HGO model does capture the behavior of waves superimposed on large deformations in which effect of fiber stretch is important. The examples in Figures 7-8 demonstrate the effects of finite deformations on wave speed.

Model parameters of both the linear elastic model and the HGO model in the reference configuration were related to the parameters of the classical, linear, elastic, orthotropic model (Young's moduli and Poisson's ratios). In its undeformed, reference configuration, the HGO model describes an orthotropic material. We note that in the reference configuration the HGO model does not exhibit shear anisotropy, which may be important in some fibrous tissues such as

muscle^{29,30}. Once it is deformed, the linearized HGO material model is no longer guaranteed to be orthotropic; the material symmetries must be determined for each specific deformed configuration.

The inverse problem (estimation of parameters from shear wave behavior, as in MRE) remains a focus of future research. Compared to estimating a single shear modulus in traditional (isotropic)

MRE, adding additional parameters will inevitably increase the difficulty of the estimation problem.

Most importantly, measurements of waves with different polarization and propagation directions will be necessary to estimate multiple material parameters. The use of different excitation techniques, such as focused ultrasound can enrich the set of shear wave data available for parameter estimation ³⁰.

V. CONCLUSION

Analytical solutions were obtained for shear wave speeds in models of soft, incompressible materials with two families of reinforcing fibers, and validated by comparison to numerical simulation. These analytical solutions relate shear wave speeds to the mechanical properties of the materials, and clarify the influence of pre-deformation (compression, shear) and fiber orientation. Improved understanding of shear wave behavior in soft, anisotropic materials will advance the prospects for non-invasive characterization of fibrous soft tissue by MRE.

ACKNOWLEDGEMENTS

NSF grant CMMI-17274212 and NIH grant R01 EB027577.

REFERENCES

- 352 ¹Kennedy P., Barnhill E., Gray C., Brown C. Beek E.J.R., Roberts N., and Greig C.A., 2019.
- 353 "Magnetic resonance elastography (MRE) shows significant reduction of thigh muscle stiffness in
- 354 healthy older adults." GeroScience. DOI: 10.1007/s11357-019-00147-2
- ²Hong S.H., Hong S.J., Yoon J.S., Oh C.H., Cha J.G., Kim H.K., and Bolster Jr B., 2016. "Magnetic
- resonance elastography (MRE) for measurement of muscle stiffness of the shoulder: feasibility with
- 357 a 3T MRI system." Acta Radiologica 57(9), pp. 1099-1106 DOI: 10.1177/0284185115571987
- 358 ³Jenkyn T.R., Ehman R.L., and An K.N., 2003. "Noninvasive muscle tension measurement using the
- novel technique of magneticresonance elastography (MRE)." J. Biomech. 36, pp. 1917-1921. DOI:
- **360** 10.1016/S0021-9290(03)00005-8
- ⁴Dzyubak B., Glaser K.J., Manduca A., and Ehman R.L., 2017. "Automated Liver Elasticity
- **362** Calculation for 3D MRE." *Proc SPIE Int Soc Opt Eng.* DOI:10.1117/12.2254476.
- ⁵Xiao G., Zhu S., Xiao X., Yan L., Yang J., and Wu G., 2017. "Comparison of Laboratory Tests,
- 364 Ultrasound, or Magnetic Resonance Elastography to Detect Fibrosis in Patients With Nonalcoholic
- 365 Fatty Liver Disease: A Meta-Analysis." Hepatology 66(5), pp. 1486-1501. DOI: 10.1002/hep.29302
- 366 ⁶Johnson C. L., McGarry M. D. J., Gharibans A. A., Weaver J. B., Paulsen K. D., Wang H., Olivero
- W. C., Sutton B. P. and Georgiadis J. G., 2013a, "Local mechanical properties of white matter
- 368 structures in the human brain" Neuroimage 79, pp. 145–52. DOI: 10.1016/j.neuroimage.2013.04.089
- ⁷Guertler C.A., Okamoto R.J., Schmidt J.L., Badachhape A.A., Johnson C.L., and Bayly P.V., 2018.
- 370 "Mechanical Properties of Porcine Brain Tissue In Vivo and Ex Vivo Estimated by MR
- 371 Elastography." *J Biomech* 69, pp.10-18. DOI: 10.1016/j.jbiomech.2018.01.016.

- 372 ⁸Guidetti M, Royston TJ. Analytical solution for converging elliptic shear wave in a bounded 373 transverse isotropic viscoelastic material with nonhomogeneous outer boundary. J Acoust Soc Am. 374 2018 Oct;144(4):2312. doi: 10.1121/1.5064372. PMID: 30404507; PMCID: PMC6197985. 375 ⁹Guidetti M, Royston TJ. Analytical solution for diverging elliptic shear wave in bounded and 376 unbounded transverse isotropic viscoelastic material with nonhomogeneous inner boundary. J 377 Acoust Soc Am. 2019 Jan;145(1):EL59. doi: 10.1121/1.5088028. PMID: 30710967; PMCID: 378 PMC6345629. 379 ¹⁰Miller R, Kolipaka A, Nash MP, Young AA. Estimation of transversely isotropic material
- properties from magnetic resonance elastography using the optimised virtual fields method. Int J

 Numer Method Biomed Eng. 2018 Jun;34(6):e2979. doi: 10.1002/cnm.2979. Epub 2018 Apr 23.

 PMID: 29528568; PMCID: PMC5993646.
- 383 ¹¹Demiray H., and Erbay H.A., 1986. "AN ORTHOTROPIC ELASTIC MODEL
 384 FORABDOMINAL AORTA." Mathematical Modelling 9(8), pp.651-658. DOI: 10.1016/0270 385 0255(87)90465-9
- Model Mechanobiol 10, pp. 613-625. DOI: 10.1007/s10237-010-0260-4

 388 ¹³Rossi S., Ruiz-Baier R., Pavarino L.F., and Quarteroni A., 2012. "Orthotropic active strain models

¹²Zou Y., and Zhang Y., 2011. "The orthotropic viscoelastic behavior of aortic elastin." Biomech

for the numerical simulation of cardiac biomechanics." Int. J. Numer. Meth. Biomed. Engng 28,

390 pp.761–788. DOI: 10.1002/cnm.2473

386

- 391 ¹⁴Caenen A., Pernot M., Peirlinck M., Mertens L., Swillens A., and Segers P., 2018. "An in silico
- framework to analyze the anisotropic shear wave mechanics in cardiac shear wave elastography."
- 393 Physics in Medicine & Biology 63 (7). DOI: 10.1088/1361-6560/aaaffe
- 394 ¹⁵Volokh K. Y., 2011, "Modeling Failure of Soft Anisotropic Materials with Application to Arteries."
- 395 J. Mecha. Behav. Biomed. Mater. 4 (8), pp. 1582–1594. DOI: 10.1016/j.jmbbm.2011.01.002
- 396 ¹⁶Shearer T., 2015, "A New Strain Energy Function for the Hyperelastic Modelling of Ligaments and
- Tendons Based on Fascicle Microstructure." J. Biomech. 48 (2), pp. 290–297. DOI:
- **398** 10.1016/j.jbiomech.2014.11.031
- 399 ¹⁷Hou Z., Okamoto R.J., and Bayly P.V., 2019. "Shear wave propagation and estimation of material
- 400 parameters in a nonlinear, fibrous material." J. Biomech. DOI: 10.1115/1.4044504
- 401 ¹⁸Fischer S., Bründler M., Sekine Y., Keshavjee S., 2002. "Solitary fibrous tumors of the pleura." The
- 402 Annals of Thoracic Surgery. 74(1), pp. 285-293. DOI: 10.1016/S0003-4975(01)03374-4
- 403 ¹⁹Rossi S., Ruiz-Baier R., Pavarino L., Quarteroni A., 2012. "Orthotropic active strain models for
- 404 the numerical simulation of cardiac biomechanics", Intel. J. for Numer. Method Biomed. Eng. 28 (6-
- 405 7), pp.761-788. DOI: 10.1002/cnm.2473²⁰Propp A., Gizzi A., Levrero-Florencio F., Ricardo
- 406 Ruiz-Baier R., 2019. "An orthotropic electro-viscoelastic model for the heart with stress-assisted
- diffusion", Biomechanics and Modeling in Mechanobiology. 19, pp. 633-659. DOI: 10.1007/s10237-
- 408 019-01237-y.
- 409 ²¹Ruiz-Baier R., Gizzi A., Loppini A., Cherubini C., and Simonetta Filippi S., 2018. "Modelling
- 410 thermo-electro-mechanical effects in orthotropic cardiac tissue". Communications in Computational
- **411** Physics (2019). DOI: 10.4208/cicp.OA-2018-0253.

- 412 ²²Ogden R. W., 1997, "Wave and vibrations," in *Non-linear elastic deformations*, Chichester :E.
- **413** Horwood, 473.
- 414 ²³Volokh K., 2016, "Plane waves in incompressible material," in *Mechanics of soft materials*, Springer
- 415 Singapore, 96. DOI: 10.1007/978-981-10-1599-1
- 416 ²⁴Birch F., 1961. "The Velocity of Compressional Waves in Rocks to 10 Kilobars, Part 2." Journal of
- 417 geophysical research, pp. 2199-2224. DOI: 10.1029/JZ066i007p02199
- 418 ²⁵Chapman C. Fundamentals of Seismic Wave Propagation. Cambridge: Cambridge University Press;
- **419** 2004
- 420 ²⁶Holzapfel G., 2000, Nonlinear Solid Mechanics: A Continuum Approach for Engineering,
- **421** Chichester: Wiley, 2000. DOI: 10.1023/A:1020843529530
- 422 ²⁷Knutsson H., Westin C. F., and Granlund G., 1994, "Local Multiscale Frequency and Bandwidth
- 423 Estimation." In Proceedings International Conference on Image Processing, ICIP, pp. 36-40. DOI:
- **424** 10.1109/ICIP.1994.413270
- 425 ²⁸Okamoto R. J., Johnson C. L., Feng Y., Georgiadis J. G., and Bayly P. V., 2014, "MRE Detection
- of Heterogeneity Using Quantitative Measures of Residual Error and Uncertainty." In Proc. SPIE
- 427 9038E, Medical Imaging 2014: Biomedical Applications in Molecular, Structural, and Functional
- 428 Imaging, San Diego, CA, 13 March 2014, 90381E, pp. 1-7. DOI: 10.1117/12.2044633
- 429 ²⁹Schmidt J. L., Tweten D. J., Benegal A. N., Walker C. H., Portnoi T. E., Okamoto R. J., Garbow J.
- 430 R., Bayly P. V., 2016, "Magnetic resonance elastography of slow and fast shear waves illuminates
- differences in shear and tensile moduli in anisotropic tissue." J. Biomech. 49(7), pp.1042-1049. DOI:
- 432 10.1016/j.jbiomech.2016.02.018

433 ³⁰Guertler C.A., Okamoto R.J., Ireland J.A., Pacia C.P., Garbow J.R., Chen H., and Bayly P.V., 2019.
434 Estimation of anisotropic material properties of soft tissue by MRI of ultrasound-induced shear
435 waves. [published online ahead of print, 2020 Jan 1]. J Biomech Eng. 2020;142(3):0310011436 03100117. doi:10.1115/1.4046127